DESIGN AND EXPERIMENTAL VERIFICATION OF SELF-PRIMING HOT AIR TEMPERATURE CHANGING DEVICE FOR GRAIN DRYER

/

粮食干燥机自吸式热风变温装置设计与试验验证

Zhao-Xin Liu[1,2], Gang Che[*1,2], Lin Wan [*1,2], Hong-chao Wang[1], Zheng-Fa Chen[1], Hao-Chen Wang[1]

[1]College of Engineering, Heilongjiang Bayi Agricultural University, Daqing / P.R.China

[2]Key Laboratory of Intelligent Agricultural Machinery Equipment in Heilongjiang Province, Daqing / P.R.China

Tel.: +86-459-13836961617; E-mile: chegang180@126.com

Corresponding author: Gang Che

DOI: https://doi.org/10.35633/inmateh-73-26

Keywords: *self-priming, variable temperature device, mutual mixing, Fluent, combination test*

ABSTRACT

During the grain drying process, in order to adjust the temperature, it is necessary to match the proportion of hot and cold air. This is the problem that the two components in the mixed gas cannot fully mix with each other in a short period of time, resulting in the problem that it takes a long time for the gas flow temperature to reach a stable value. Based on the process and technical requirements of the dryer, a self-priming hot air temperature changing device suitable for the dryer was designed. The two gas components used to improve the variable temperature ratio of the dryer are fully mixed with each other in a short time and a short distance, thereby reducing the loss caused by the food not reaching safe moisture. Based on Bernoulli's principle and the basic theory of airflow mixing in fluid dynamics, a mathematical model of airflow mixing in the constriction section of the main pipeline was established. Fluent was used to numerically simulate the distribution of uniform mixing distance and temperature field in the necking section. The results show that the mixing uniformity in the necking section reaches 75%-80%, which effectively improves the mixing efficiency. A self-priming hot air temperature change device test bench developed independently was used, and the quadratic orthogonal rotation combined test method was used for parameter optimization. Design-Expert.V8.0.6.1 was used for analysis and testing, and the regression equation and response surface were obtained to analyze the effects. Interaction between factors to determine the best combination of optimization parameters: when the number of air inlet pipes is 3.16, the incision axial angle is 27.6°, the temperature difference is 43.5°C, and the pipe diameter is 23.8 mm, the post-mixing temperature is 50.93°C, and the mixing distance is uniform is 39.33 mm. The test results are consistent with the optimization results. The self-priming hot air temperature changing device of the dryer has certain practical application value.

摘要

在谷物干燥过程中，为调节温度，需要根据冷热空气的比例配比。为混合气体中的两种组分在短时间内无法充分相互混合，导致气流温度达到稳定值需要较长时间的问题。基于干燥机的工艺与技术要求，设计了一种适用于干燥机自吸式热风变温装置。用于提高干燥机变温配比的两种气体组分短时间、短距离的充分相互混合，进而减少粮食未达到安全水分造成损失。基于流体动力学中伯努利原理和气流混和的基本理论，建立了在主管道缩颈段的气流混配的数学模型。运用 Fluent 对缩颈段内混合均匀距离和温度场的分布情况进行了数值模拟。结果表明：在缩颈段混合均匀度达到 75～80%，有效的提高了混合效率。采用自主研制的自吸式热风变温装置试验台，应用二次正交旋转组合试验方法进行参数优化，运用 Design-Expert.V8.0.6.1 进行分析检验，得到回归方程和响应曲面，分析各影响因素之间的交互作用，以确定优化参数最佳组合：当进气管数量为 3.16、切口轴向角 27.6°、温差 43.5°C、导管直径 23.8mm 时混后温度为 50.93°C，混合均匀距离为 39.33mm，试验结果与优化结果相符合，干燥机自吸式热风变温装置具有一定的实际应用价值。

INTRODUCTION

According to the National Bureau of Statistics' announcement on grain output data in 2022, the country's total grain output was 686.53 million tons (1,373.1 billion kilograms), an increase of 3.68 million tons (7.4 billion kilograms) compared with 2021, an increase of 0.5%. Among them, grain output is 633.24 million tons (1,266.5 billion catties), an increase of 490,000 tons (1 billion catties) compared with 2021. However, every year due to climate reasons, the drying time is not enough to reach safe moisture, resulting in losses of up to 5% of the total output. Therefore, it is crucial to reduce the temperature uniformity time of the mixed airflow and accurately control it (*Chen et al., 2020*).

Rice drying usually uses two drying methods: traditional natural drying and mechanical drying. The traditional natural drying method is easily affected by various factors such as climate and site. In recent years, the sales of drying devices have increased year by year, so research on the precise adjustment of rice drying devices is very necessary. In terms of drying technology research *Jiang and Liu* (*2009*) tested two drying processes, low constant temperature drying and variable temperature drying, on a batch circulation rice dryer; domestic scholar (*Liu et al., 2023*) studied the technology and performance of the rice variable temperature homogeneous drying device; it was conducted experimental research on the variable temperature and quality-preserving drying technology and control process of rice (*Li, 2019*); in terms of mixed flow investigation, research by Ahri Ozkan (*Fahri et al., 2006*) and others has verified that the Venturi effect can significantly increase the solubility of oxygen in water. Song Kangkang used the CFD method to analyze the solid-liquid two-phase flow field of the SH20 mixed-discharge integrated device, and improved the design of the device (*Song et al., 2023*). Therefore, a stable temperature changing device is an important prerequisite for ensuring drying quality (*Hang et al., 2014*). The temperature-changing mechanical system of the dryer is mostly separated from the cold air inlet and the hot air inlet. Cold and hot air fan blowers are used to work at the same time to control temperature changes. There is room for improvement in both its energy consumption and real-time temperature changing level.

MATERIALS AND METHODS

Self-priming hot air temperature changing device and its working principle

The self-priming hot air temperature changing device includes an air volume hot air inlet connected to a heating fan blower, and a mixer outlet connected to a drying device. The main pipeline consists of an inlet section, a constriction section and a diffusion section, as shown in Fig. 2. The fan blower is shown in Fig. 1. The fan blower is a hot air supply device. The tail of the air inlet pipe is placed in the constriction section. The hot air in the main pipe passes through the constriction section and creates a pressure difference with the atmospheric pressure, causing the air to enter from the air inlet pipe and mix with the air in the main pipe for cooling. When the temperature required for drying needs to be changed, the sliding plate of the variable temperature adjustment device is driven by the drive motor and forms staggered openings with the fixed plate to control the amount of air entering and thereby control the temperature.

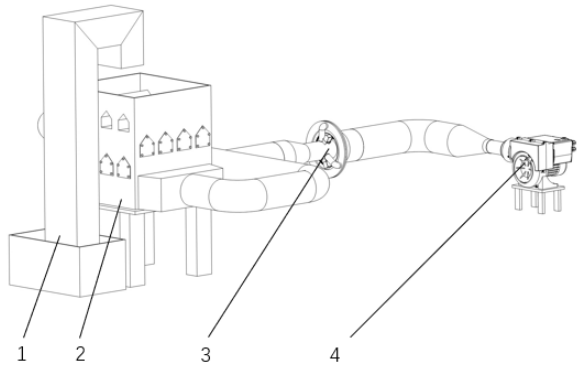

Fig. 1 - Variable temperature drying test bench
1. Elevator; 2. Dryer; 3. Temperature changing device; 4. Heating fan blower;

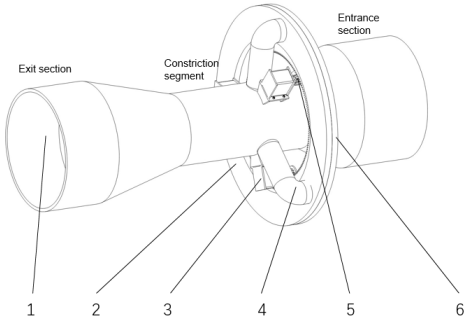

Fig. 2 - Self-priming hot air temperature changing device
1. Main pipe; 2. Fixed plate; 3. Drive motor; 4. Inlet pipe; 5. Drive gear; 6. Sliding plate

Design calculation of air inlet size

During the design and research of hot and cold air flow mixing devices, the principle of hot and cold air ratio is that hot and cold air are mixed according to a certain ratio, and a new equilibrium state is reached after mixed flow and heat transfer within a certain distance. The temperature changing device in this article adopts negative pressure self-priming air inlet. The air flow mixing angle is analyzed as intersecting air flow mixing. During the mixing process, the cold air enters the main pipe through the air inlet pipe. When the cold air passes through the tail of the air inlet pipe, it is cold air due to its guiding role. When the spiral enters through an oblique cut, entrainment is formed inside the airflow, the expansion angle increases, and the mixing becomes more complete, thereby forming a uniform airflow, that is, uniform mixing can be achieved within a short distance. The area of the near-air opening and closing section of the cold air is shown in Fig. 2:

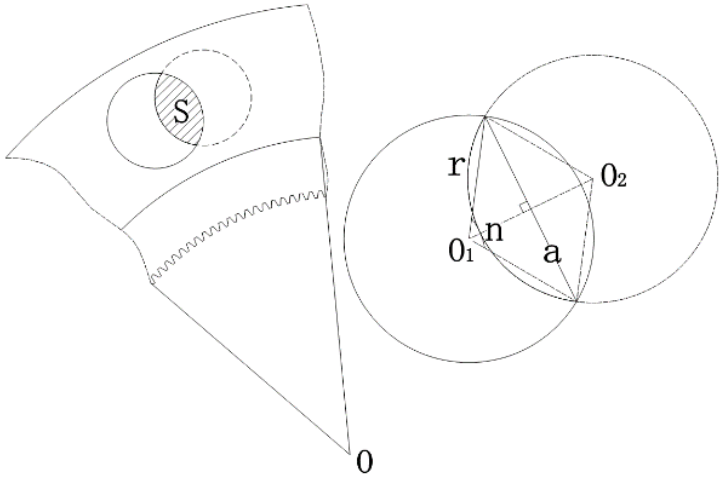

Fig. 3 - Close air opening and closing section

$$a = 2rsinn \tag{1}$$

$$S \approx r^2\left(0.017n - sinn\sqrt{1 - sin^2 n}\right) \tag{2}$$

where:

r is the radius of the intake pipe, [mm]; n is the sector angle, [°] ; a is the chord length, [mm] ;Bernoulli's equation for spiral flow is:

$$\frac{\gamma}{\gamma-1}\frac{p}{\rho} + \frac{1}{2}V^2 = C(n) \tag{3}$$

where:

γ is the helix angle, [°] ; p is pressure, [Pa] ; ρ is density, [kg/m^3] ; V is the flow rate, [m/s] ;$C(n)$ is a constant ;

The amount of cold air proportioned through the intake pipe per unit time and the cross-sectional air volume of the hot air in the constriction section of the main pipe are equal to the mixed cross-sectional air volume. According to the above equations 1, 2, and 3, the expression is:

$$V_3\pi R^2 + V_2 S = V_m\pi R^2 \tag{4}$$

where:

R is the radius of the necked section pipe, [mm]; V_3 is the flow velocity of the necked section pipeline, [m/s]; V_2 is the flow rate of cold air into the pipe, [m/s]; S is the cold air inlet area, [m^2]; V_m is the wind speed after mixing, [m/s];

In order to meet the requirements of drying air volume adjustment and to obtain the minimum hot air temperature, it is assumed that the temperature fluctuation is ±1°C, the hot air temperature is 40~70°C, and the ambient temperature is 20. Determining the wind speed of the main duct by changing the wind speed and then the pressure of the necked section has no effect on its indicators. Determine the structural parameters according to the changes in the temperature of the main duct. The combined equations 1, 2, and 3 yield that the opening area of the main duct is approximately no more than 0.0023 m^2, combined with the size of the main pipeline necking section, determine the circular section radius to be 16 mm, the number is 3 and they are evenly distributed in the main pipeline necking section.

Intake pipe design

The intake pipe is installed in the necked section of the main pipe. A circular hole is set 135 mm from the beginning of the necked section. The tail of the intake pipe is placed in the circular hole and has a beveled arc opening and a horseshoe shape. The tail of the intake pipe has both a radial angle α and an axial angle β of the incision with the intake pipe itself, as shown in Fig. 4.The tail of the inlet pipe in the necked section of the main pipe is arranged in a spiral inside the pipe, so that when the cold air passes through the tail of the inlet pipe, the cold air enters through a spiral bevel due to its guiding function, and the air flow is entrained inside, and the expansion angle increases. At the same time, the hot gas in the main pipe also has a certain spiral guide, and its mixing is more uniform, thereby forming a uniform mixed gas. And the tail of the intake pipe faces the direction of the main pipe airflow, which prevents backflow.

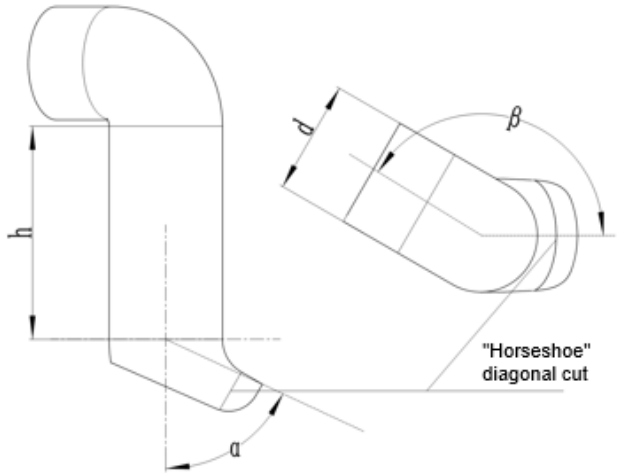

Fig. 4 - Intake pipe structure diagram

Design and optimization of adjusting plate

The air volume adjustment device consists of a fixed plate and a sliding plate. The fixed plate and the sliding plate are respectively provided with circular holes in the center. An internal ring gear is arranged on the inner circumference of the sliding plate. The fixed plate and the sliding plate are evenly provided with holes along their circumferences. The fixed plate is fixedly connected with the head of the air intake pipe. When the temperature required for drying needs to be changed, the sliding plate of the air volume adjustment device is driven by the motor and forms staggered openings with the fixed plate to control the amount of air entering and thereby control the temperature.

Since the fixed plate and the sliding plate are installed closely, an annular slideway is provided on the inner circumference of the opposite fixed plate, and an annular slide rail is provided on the inner end surface of the sliding plate. The annular slideway and the annular slide rail fit together. The installation enables the sliding disc to rotate on the surface of the fixed disc.

Since the design of friction on the slide rail is relatively complex, formula 5 for calculating the radial toroidal friction moment is:

$$M = \int_{R_2}^{R_1} dM = \frac{2}{3}\mu mg\left(R_1{}^1 - R_2{}^2\right) \quad (5)$$

$$S \approx 3\pi r^2 \quad (6)$$

$$R_1 - R_2 > 2r \quad (7)$$

where: R_1 is the radius of the outer circular surface, [mm]; R_2 is the radius of the inner circular surface, [mm]; μ is the friction coefficient of the sliding disk material; m is the mass of the sliding disk, [kg]; g is the gravity acceleration, [m/s^2]; S is the cold air inlet Area, [m^2]; r is the radius of the intake pipe, [mm];

Through formulas 5, 6, and 7, the equation is calculated: in order to ensure that the material of the adjustment plate is unique, (polyamide) material was selected for 3D printing in the test, which is stable and reliable while minimizing the distance between the inner and outer slideways as much as possible. The optimal structure obtained is that the radius of the inner slideway R_1 is approximately 247.5 mm, and the radius of the outer slideway R_2 is approximately 332.5 mm.

NUMERICAL SIMULATION ANALYSIS

Build mathematical models

The solver in Fluent software is used to perform simulation calculations. The continuity equation in the Cartesian coordinate system is Formula 8:

$$\frac{\partial}{\partial x_i}(\rho u_i) = 0 \tag{8}$$

The momentum equation is equation 9:

$$\frac{\partial}{\partial x_i}(\rho u_i u_j) = \frac{\partial}{x_i}\left[\mu_e\left(\frac{\partial u_i}{\partial x_j} + \frac{\partial u_j}{\partial x_i}\right)\right] + \rho g_j - \frac{\partial}{\partial x_j}\left(p + \frac{2}{3}\mu_e \frac{\partial u_i}{\partial x_i}\right) \tag{9}$$

The energy equation is equation 10:

$$\frac{\partial}{\partial x_i}(\rho u_i i) = \frac{\partial}{\partial x_i}\left[\mu\left(\frac{1}{Pr} + \frac{\frac{\mu_i}{\mu}}{Pr_t}\right)\frac{\partial i}{\partial x_i}\right] \tag{10}$$

where:

ρ is density, [kg/m^3]; u is velocity, [m/s]; p is pressure, [Pa]; μ_e is effective viscosity; μ_e=μ+μ_t; μ is molecular viscosity; μ_t is turbulent viscosity; i is specific enthalpy; Pr is molecular Prandtl Number; Pr=$\mu C_p/\lambda$; C_p is specific constant pressure heat capacity; λ is thermal conductivity; turbulent Prandtl number Pr_t=$\mu_t C_p t/\lambda_t$; λ_t is eddy flow thermal conductivity; in the calculation process Pr_t is usually set to 0.85;

Since the fluid domain model is relatively simple, the simple-C solver is selected for solution. Commonly used turbulence models in Fluent include Standard, RNG, Realizable, etc. Considering the existence of rotating uniform shear flow, Realizable's k-epsilon model is selected to simulate airflow mixing. Turbulent viscosity is calculated as equation 11:

$$\mu_t = \rho C_\mu \frac{k^2}{\varepsilon} \tag{11}$$

The Realizable k-epsilon turbulent kinetic energy transport equation is equation 12:

$$\frac{\partial \rho}{\partial t}(\rho k) + \frac{\partial}{\partial x_i}(\rho k \mu_i) = \frac{\partial}{\partial x_j}\left[\left(\mu + \frac{\mu}{\partial_k}\right)\frac{\partial k}{\partial x_j}\right] + G_k + G_b - \rho\varepsilon - Y_m + S_k) \tag{12}$$

The Realizable k-epsilon turbulent dissipation rate transport equation is equation 13:

$$\frac{\partial}{\partial t}(\rho\varepsilon) + \frac{\partial}{\partial x_j}(\rho\varepsilon\mu_j) = \frac{\partial}{\partial x_j}\left[\left(\mu + \frac{\mu}{\partial_k}\right)\frac{\partial k}{\partial x_j}\right] + \rho C_1 S\varepsilon - \rho C_2 \frac{\varepsilon^2}{\kappa + \sqrt{\nu\varepsilon}} - C_{1\varepsilon}\frac{\varepsilon}{k}C_{3\varepsilon}G_b + S_\varepsilon \tag{13}$$

where:

G_k is the generation of turbulent kinetic energy caused by the average velocity gradient; G_b is the generation of turbulent kinetic energy caused by buoyancy; Y_m is the effect of the pulsating expansion of compressible turbulent flow on the total dissipation rate; $C_{1\varepsilon}$ $C_{2\varepsilon}$ $C_{3\varepsilon}$ are empirical constants; the default values are $C_{1\varepsilon}$=1.44, $C_{2\varepsilon}$=1.92, $C_{3\varepsilon}$=0.09; σ_k, σ_ε are the Prandtl coefficients corresponding to turbulent kinetic energy and turbulent kinetic energy dissipation rate respectively; β is thermal expansion Coefficient; M_t is the turbulent Mach number; a is the speed of sound, [m/s];

Setting of boundary conditions

Taking the self-priming hot air temperature changing device as the prototype, a simplified three-dimensional model of the fluid domain was established and imported into ANSYS, and the fluid domain was divided into volume meshes (*Papkov et al., 2023*). The hot air flow passes through the inlet section, constriction section, and diffusion section in sequence. When passing through the constriction section, the pressure difference between the constriction section and the atmospheric pressure causes the air to enter from the air inlet pipe and mix with the main pipe air to achieve cooling. The mixed gas enters the dryer inlet duct through the inlet section.

In order to make the simulation close to reality, this paper uses the steady-state flow field for simulation. The two-phase flow medium is air, and SWF is selected as the wall function.

The fluid domain model has an arc wall, so a curvature correction coefficient is added to improve the authenticity of the model. During the simulation process, the inlet section port is set to the velocity inlet gas flow rate of 5m/s and the temperature is set to 60°C. The inlet pipe port of the constriction section is set to the pressure inlet. Its initial gauge pressure is set to 0 MPa and the temperature is set to 20°C. The diffusion section port is set to the pressure outlet gauge, the pressure is set to 0MPa, and the temperature is set to 20°C.

Numerical simulation analysis of necking section

When the mixed gas passes through the constriction section, the two components, which have low pressure and fast flow rate, do not mix with each other. Therefore, the length of the constriction section is 135 mm at the beginning of the constriction section and its length is 60 mm for temperature monitoring (*Gao et al., 2018; Han et al., 2023; Kavga et al., 2023; Liu et al., 2023*). 13 temperature monitoring points are evenly selected in each section. Point 5 is shown in Fig. 5 for instantaneous monitoring, and the temperature of each cross-section monitoring point is shown in Fig. 6.

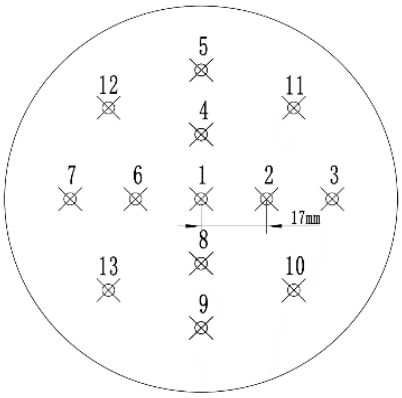

Fig. 5 - Section monitoring selected points

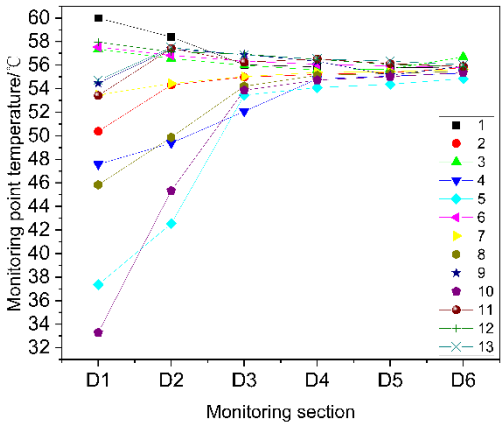

Fig. 6 - Temperature point and line diagram of cross-section monitoring points

The length of the necking section is 60 mm at 135 mm from the beginning, and monitoring is performed every 10 mm. The relationship between the monitoring sections (a, b, c, d, e, f) and temperature is shown in Fig. 7. The results show that: From a to b, the gas is still in stratified flow. From b to f, the temperature tends to be between 42°C and 58°C and gradually becomes stable. The temperature changes at each monitoring point in the b to c section are relatively large according to *Gao and Jiang* (*2018*). The temperature changes at each monitoring point in section e ~ f are relatively small; the temperature changes around monitoring points 4 and 5, and between 13, 9 and 10 are particularly obvious. The cloud images of each section are shown in Fig. 7.

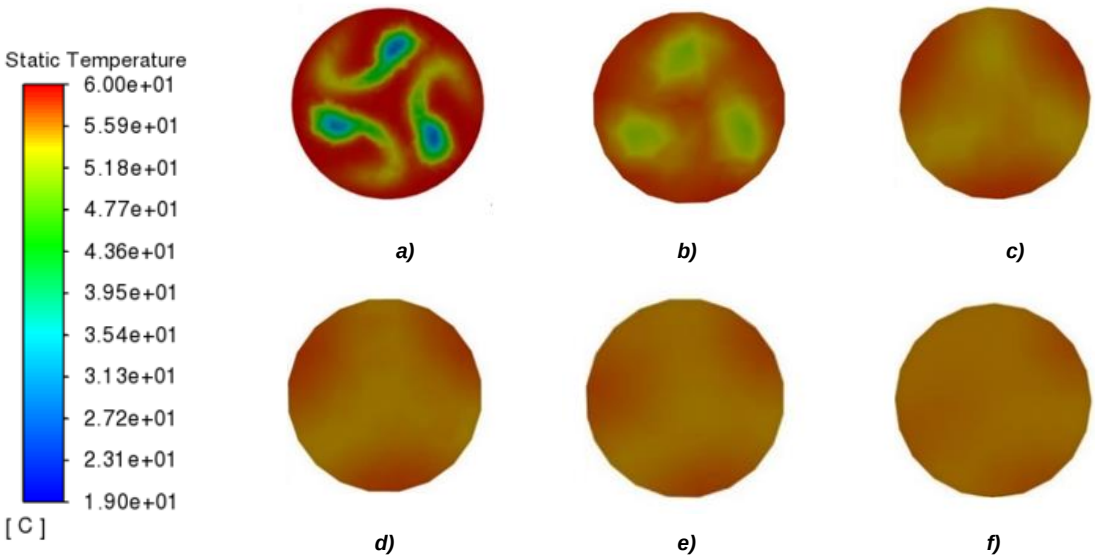

Fig. 7- Cross-section temperature distribution cloud chart

Experimental analysis of the impact of various factors on experimental indicators

When the number of intake pipes is determined to be 3, the diameter of the intake pipe is 32 mm, the flow velocity of the main pipe is 5 m/s, the temperature difference between hot and cold air is 40°C and other parameters are certain, the number of axial angles of the incisions at the end of the intake pipe is set to 15°, 30°, and 45°, thereby obtaining a graph of the temperature after mixing of hot and cold air, the uniform distance of mixing, and the axial angle of the incision at the end of the intake pipe, as shown in Fig. 8.

It can be seen from the fig. that the axial angle of the incision has a significant impact on the uniform mixing distance, but the influence on the temperature is not significant. When the axial angle of the incision is set to 15°, the distance for uniform air flow mixing is 45 ~ 50 mm. When the axial angle is set to 30°, the distance required for the airflow to be evenly mixed is 40 ~ 42 mm. When the axial angle of the incision is set to 45°, the distance required for the airflow to be evenly mixed is 57 ~ 62 mm. When the axial angle of the incision is 30°, the mixing distance is relatively short. When the axial angle of the incision is smaller, the torsional force on the airflow is smaller, and the bevel angle of the cold air entering the hot air is smaller, and the mixing distance is longer. When the axial angle of the incision is larger, the torsional force on the airflow is greater, and the oblique angle at which the cold air enters the hot air is larger, causing the cold air to enter the surface layer of the hot air in the main pipe, which is not conducive to the heat conduction of the gas, making the mixing distance longer.

Under the condition that the number of air inlet pipes is 3, the pipe diameter is 32 mm, the axial angle of the incision is 30°, the flow rate of the main pipe is 5 m/s and other parameters are certain, the temperature difference between the hot and cold air is set to 20°C, 40°C, and 60°C respectively, thus obtaining the curve of the temperature after mixing of hot and cold air and the mixing uniform distance and temperature difference, as shown in Fig. 9. It can be seen from the fig. that the temperature difference has a significant impact on the mixing temperature. When the temperature difference is set to 20°C, the temperature at which the airflow is evenly mixed is 58 ~ 58.5°C. When the temperature difference is set at 40°C, the temperature at which the airflow is evenly mixed is 56 ~ 57°C. When the temperature difference is set to 60°C, the temperature at which the airflow is evenly mixed is 53 ~ 55°C. Therefore, as the temperature difference expands, the temperature after mixing is lower, and the lower the temperature can be adjusted. The larger the range, the more accurate real-time temperature variable mixing can be achieved.

When it is determined that the diameter of the air inlet pipe is 32 mm, the axial angle of the incision is 30°, the flow rate of the main pipe is 5 m/s, the number of air inlet pipes is 1, 3, 5, and other parameters as in the test are certain, thus obtaining the curve diagram of the temperature after mixing of hot and cold air, the uniform distance of mixing and the number of air intake pipes, as shown in Fig. 10.

It can be seen from the fig. that the number of air inlet pipes has a significant impact on the mixing temperature and uniform mixing distance. When the number of air inlet pipes is set to 1, the temperature at which the air flow is evenly mixed is 57 ~ 58°C. When the number of air inlet pipes is set to 5, the temperature at which the air flow is evenly mixed is 58 ~ 59°C. Therefore, when the number of pipes is 1, the temperature of the mixed air flow is the lowest, the adjustable range is the largest to meet greater temperature changing needs. When the number of air inlet pipes is set to 1, the distance for uniform air flow mixing is 125 ~ 150 mm. When the number of air inlet pipes is set to 3, the distance for uniform air flow mixing is 40 ~ 42 mm. When the number of air inlet pipes is set to 5, the temperature for uniform air flow mixing is 35 ~ 37 mm, so as the number of tubes increases, the distance for uniform airflow mixing becomes shorter.

After determining that the number of air inlet pipes is 3, the axial angle of the incision is 30°, the flow rate of the main pipe is 5 m/s, and other parameters are certain, the diameter of the air inlet pipes is set to 22 mm, 32 mm, and 42 mm respectively, so as to obtain a mixture of hot and cold air. The curves of the temperature after mixing, the mixing uniform distance and the diameter of the air inlet pipe are shown in Fig. 11.

It can be seen from the fig. that the diameter of the air inlet pipe has a significant impact on the mixing temperature. When the pipe diameter is 22 mm, the temperature at which the airflow is evenly mixed is 57 ~ 57.5°C. When the pipe diameter is 32 mm, the temperature at which the airflow is evenly mixed is 56 ~ 57°C. When the pipe diameter is 42 mm, the temperature at which the air flow is evenly mixed is 55.5 ~ 56°C. Therefore, as the pipe diameter expands, the temperature after mixing is lower, and the lower the temperature can be adjusted. The larger it is, the more accurate real-time temperature-changing mixing can be achieved.

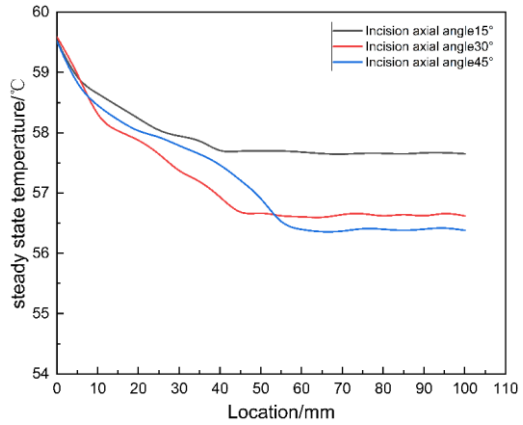

Fig. 8 - Effect of axial angle of incision on performance indicators

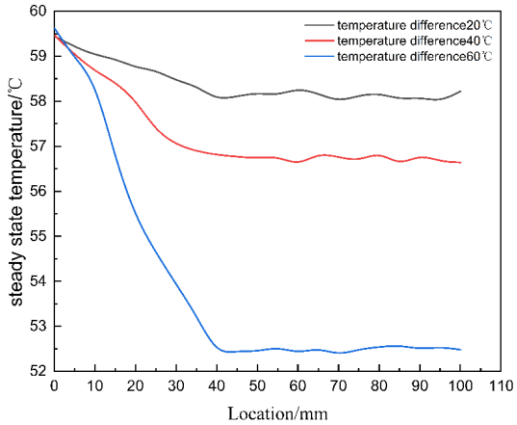

Fig. 9 - Effect of temperature difference angle on performance indicators

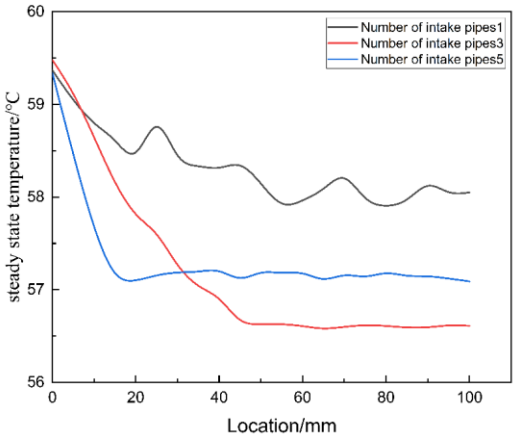

Fig. 10 - The impact of the number of intake pipes on performance indicators

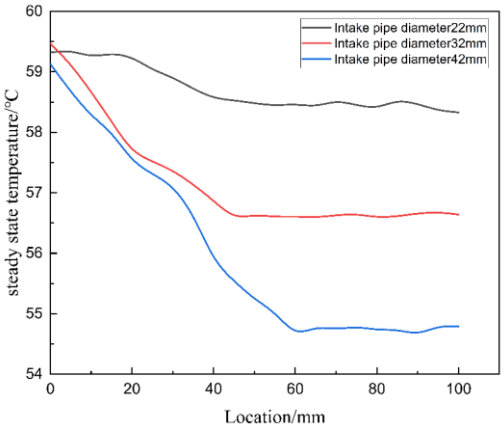

Fig. 11 - Effect of intake pipe diameter on performance indicators

RESULTS

Experimental design and response analysis

Taking the number of air inlet pipes X_1, the axial angle of the incision X_2, the temperature difference X_3 and the diameter of the air inlet pipe X_4 of the variable temperature device as test factors, the uniform mixing distance Y_1 and the mixing temperature Y_2 as optimization indicators, a quadratic orthogonal rotation of four factors and five levels was used. Through the combined design test, the optimized structure of each working component on the mixing device was determined, and the test factor range and level coding table were compiled, as shown in Table 1.

Table 1

Factor Level Coding

Coding	Number of intake pipes X_1 [PCS]	Incision axial angle X_2 [°]	Temperature difference X_3 [℃]	Intake pipe diameter X_4 [mm]
+2	5	60	50	42
+1	4	45	40	37
0	3	30	30	32
-1	2	15	20	27
-2	1	0	10	22
	1	15	10	5

Table 2

Results of the trial data

Coding	Experimental factors				Test indicators	
	Number of intake pipes X_1 [PCS]	Incision axial angle X_2 [°]	Temperature difference X3 [℃]	Intake pipe diameter X_4 [mm]	Mixing uniform distance Y_1 [mm]	Mixing temperature Y_2 [℃]
1	-1	-1	-1	-1	54.72	58.25
2	1	-1	-1	-1	47.23	56.44
3	-1	1	-1	-1	57.46	55.58
4	1	1	-1	-1	57.71	56.09
5	-1	-1	1	-1	48.71	58.82
6	1	-1	1	-1	34.32	53.37
7	-1	1	1	-1	58.78	56.48
8	1	1	1	-1	46.31	53.73
9	-1	-1	-1	1	46.27	58.41
10	1	-1	-1	1	41.22	57.62
11	-1	1	-1	1	47.04	57.2
12	1	1	-1	1	44.02	57.96
13	-1	-1	1	1	48.77	56.31
14	1	-1	1	1	36.87	52.59
15	-1	1	1	1	47.85	56.28
16	1	1	1	1	39.99	55.2
17	-2	0	0	0	57.34	56.38
18	2	0	0	0	41.89	53.44
19	0	-2	0	0	38.18	57.78
20	0	2	0	0	55.26	55.3
21	0	0	-2	0	50.06	58.87
22	0	0	2	0	43.03	56.7
23	0	0	0	-2	51.33	56.54
24	0	0	0	2	37.41	58.76
25	0	0	0	0	55.71	50.28
26	0	0	0	0	52.97	51.45
27	0	0	0	0	52.97	51.45
28	0	0	0	0	53.25	51.36
29	0	0	0	0	51.61	52.04
30	0	0	0	0	52.51	52.09

As shown in Table 2, the model of mixed uniform distance P<0.01 indicates that the model is statistically significant, and the test result of the lack of fit item is P=0.2635>0.05, which is an insignificant item, indicating that the fit of the regression equation is good and has practical significance. The uniform mixing temperature model P<0.01 indicates that the model is statistically significant, and the test result of the lack of fit item is P=0.5052>0.05, which is an insignificant item, indicating that the regression equation has good fitting properties and has practical significance. After eliminating non-influencing factors, the regression equations of uniform mixing distance and uniform mixing temperature are obtained, which are divided into equation s 14 and 15:

$$Y_1 = 53.16 - 3.98X_1 + 3.16xX_2 - 2.01X_3 - 3.37X_4 + 0.99X_1X_2 - 1.99X_1X_3 + 0.42X_1x_4 + 0.50X_2X_3 - 1.88X_2X_4 + 1.50X_3X_4 - 0.80{X_1}^2 - 1.53{X_2}^2 - 1.57{X_3}^2 - 2.11{X_4}^2 \quad (14)$$

$$Y_2 = 51.45 - 0.84X_1 - 0.34X_2 - 0.80X_3 + 0.30X_4 + 0.58X_1X_2 - 0.73X_1X_3 + 0.39X_1X_4 + 0.28X_2X_3 + 0.42X_2X_4 - 0.43X_3X_4 - 0.79{X_1}^2 + 1.20{X_2}^2 + 1.51{X_3}^2 + 1.48{X_4}^2 \quad (15)$$

The response surface of the interaction between the number of inlet pipes and the axial angle of the incisions on the uniform mixing distance can be seen from Fig. 12a. When the number of inlet pipes remains unchanged, as the axial angle of the incisions increases, the uniform mixing distance first increases and then there is a decreasing trend; when the axial angle of the incision remains unchanged, the number of air inlet pipes increases, the uniform mixing distance shows a decreasing trend, the overall trend changes are more obvious and the range of change is smaller, and the overall trend becomes stable.

The response surface of the interaction between the number of air inlet pipes and the temperature difference on the uniform mixing distance can be seen from Fig. 12b: when the number of air inlet pipes remains unchanged, as the temperature difference increases, the uniform mixing distance first increases and then decreases; When the temperature difference remains unchanged, as the number of air inlet pipes increases, the uniform mixing distance first increases and then decreases. The overall trend changes relatively smoothly and has a small range of change.

The response surface of the interaction between the axial angle of the incision and the diameter of the inlet pipe on the uniform mixing distance can be seen from Fig. 12c: when the axial angle of the incision remains unchanged, as the diameter of the inlet pipe increases, the uniform distance of mixing decreases. Small trend: when the diameter of the inlet pipe remains unchanged, as the axial angle of the incision increases, the uniform mixing distance first increases and then decreases. The overall trend changes are more obvious and the range of changes is larger.

The response surface of the interaction between the temperature difference and the diameter of the air inlet pipe on the uniform mixing distance can be seen from Fig. 12d: when the diameter of the air inlet pipe remains unchanged, as the temperature difference increases, the uniform mixing distance shows a decreasing trend; when the temperature difference is constant, with the increase of the diameter of the inlet pipe, the mixing uniform distance increases first and then decreases, and the overall trend changes more obviously and the change range is larger.

The response surface of the interaction between the number of air inlet pipes and the axial angle of the incision on the mixing temperature can be seen from Fig. 12e: It can be seen from the fig. that when the number of air inlet pipes remains unchanged, as the axial angle of the incision increases, the mixing temperature increases first, the trend decreases and then increases; when the axial angle of the incision remains unchanged, the number of intake pipes increases, and the mixing temperature first decreases and then increases. The overall trend changes are more obvious and the range of changes is smaller, and the overall trend is stable.

The response surface of the interaction between the number of air inlet pipes and the temperature difference on the mixing temperature can be seen from Fig. 12f: when the number of air inlet pipes remains unchanged, as the temperature difference increases, the mixing temperature first decreases and then increases. When the temperature difference remains unchanged, as the number of air inlet pipes increases, the mixing temperature first decreases and then increases. The overall trend changes relatively smoothly and has a small range of change.

The response surface of the interaction between the axial angle of the incision and the diameter of the tube on the mixing temperature can be seen from Fig. 12g: when the axial angle of the incision remains unchanged, as the diameter of the inlet tube increases, the mixing temperature first decreases, then increases; when the diameter of the inlet pipe remains unchanged, as the axial angle of the incision increases, the mixing temperature shows a trend of increasing first. The overall trend changes are more obvious and the range of changes is larger.

The response surface of the interaction between temperature difference and pipe diameter on the mixing temperature can be seen from Fig.12h: when the diameter of the inlet pipe remains unchanged, as the temperature difference increases, the mixing temperature shows a decreasing trend; when the temperature difference is constant, with the increase of the diameter of the inlet pipe, the mixing temperature increases first and then decreases, and the overall trend changes more obviously and the change range is larger.

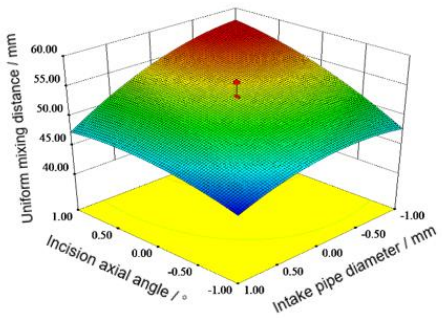

a) Effects of the axial angle of the incision and the diameter of the inlet pipe on the uniform mixing distance

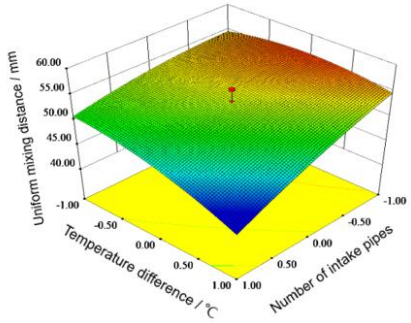

b) Effect of temperature difference and number of air inlet pipes on uniform mixing distance

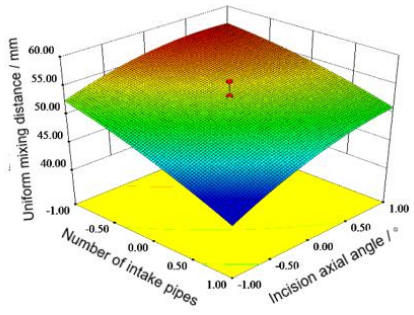

c) Effect of the number of air inlet pipes and the axial angle of the incision on the uniform mixing distance

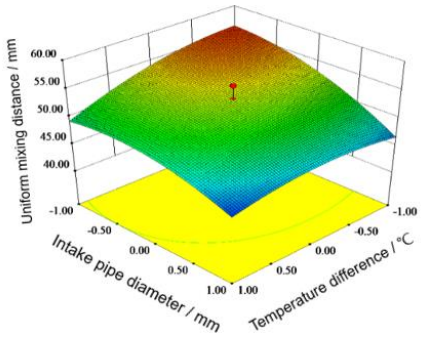

d) Effects of intake pipe diameter and temperature difference on uniform mixing distance

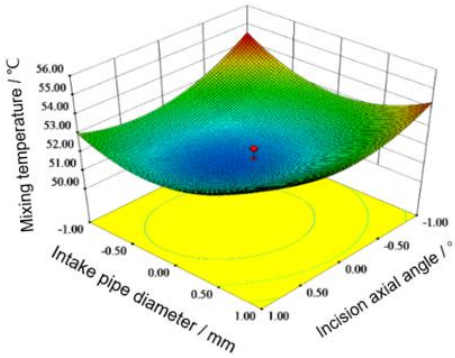

e) Inlet pipe diameter and cut axial angle on mixing temperature

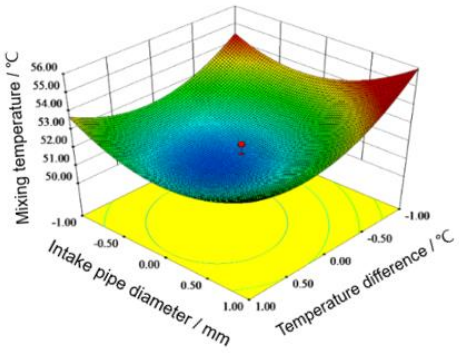

f) Intake pipe diameter and temperature difference on mixing temperature

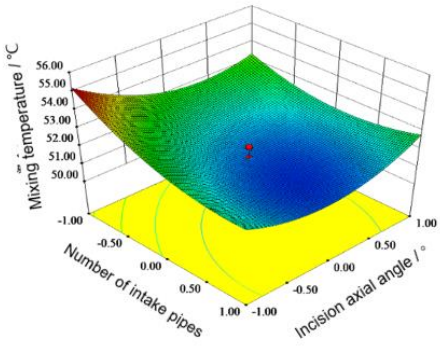

g) Effect of the number of intake pipes and the axial angle of the incision on the mixing temperature

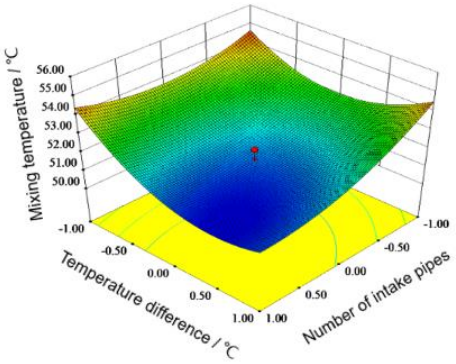

h) Effect of the number of intake pipes and temperature difference on the mixing temperature

Fig. 12 - The impact of interactive factors on test indicators

Test equipment and methods

The equipment required for the test bench includes (Keshun Measurement and Control) temperature and humidity transmitter, (Jianda Nishina) wind speed sensor, tape measure and other test devices. The test location was conducted in the Intelligent Drying Laboratory of Heilongjiang Bayi Agricultural University. The temperature variable device was connected to the fan blower and drying device as shown in Fig.13. Before the test, three (Keshun Measurement and Control) temperature and humidity transmitters are evenly installed at the fan blower pipe outlet. When the temperature is stable, the average temperature of the three points is taken. Set up 3 (Jianda Nishina) wind speed sensors evenly. When the wind speed is stable, take the average of 3 wind speeds. The average temperature of the experimental environment is about 10°C. Monitoring is performed every 10 mm after the air inlet duct, a total of 10 times, with a total length of 100 mm. Select 5 points evenly in each section, repeat 5 times, and process the data collected each time.

Fig. 13 - Variable temperature drying test bench

Test data optimization and verification

Using Design-Expert 8.0.6 software to optimize, select three sets of optimization data and take the average value to obtain the post-mixing temperature of 50.93 when the number of air intake pipes is 3.16, the axial angle of the incision is 27.6°, the temperature difference is 43.5°C, and the diameter of the intake pipe is 23.8 mm, the mixing uniform distance is 39.33 mm. During the experimental verification process, the number of air inlet pipes was selected to be 3, the axial angle of the incision was 27°, the temperature difference was 45°C, the diameter of the air inlet pipe was 24 mm, and monitoring was performed every 15 mm after the air inlet pipe. Repeat the test 5 times to take the average, the result is that the temperature after mixing is 51.24°C, and the uniform mixing distance is 38.94 mm. A system of objective equations and constraint equations:

$$\begin{cases} minY_1 \\ minY_2 \\ \begin{cases} 1 \le X_1 \le 5 \\ 0° \le X_2 \le 60° \\ 10°C \le X_3 \le 50°C \\ 22mm \le X_4 \le 42mm \\ 0 \le Y_1(X_1, X_2, X_3, X_4) \le 1 \\ 0 \le Y_2(X_1, X_2, X_3, X_4) \le 1 \end{cases} \end{cases} \tag{16}$$

Relative error:

$$\delta = \frac{\Delta}{L} \times 100\% \tag{17}$$

where:

Δ absolute error; L truth value.

Table 3

Optimization and test results

Project	Mixing temperature [℃]	Uniform mixing distance [mm]
Optimization Results	50.93	39.33
Actual results	51.24	38.94
Relative error [%]	6.04	9.76

It can be seen from Table 3 that there is not much difference between the optimized value and the experimental value, and all indicators are at a relatively good level.

CONCLUSIONS

Using the principle of theoretical mechanics friction torque to analyze the friction of the slide rail in the air volume adjustment device, the results show that while ensuring that the material is unique, stable and reliable, the distance between the inner and outer slides should be minimized as much as possible to obtain the optimal. The structure has an inner slide radius R_1 of approximately 247.5 mm, and an outer slide radius R_2 of approximately 332.5 mm. Using Bernoulli's principle of fluid dynamics and the basic theory of airflow mixing to combine mathematical equations, the results show that the pipe opening area is approximately no more than 0.0023 m^2. Combined with the size of the main pipe necking section, the circular cross-section radius is determined to be 16 mm.

Fluent was used to numerically simulate the distribution of uniform mixing distance and temperature field in the necking section. Taking the uniform mixing distance and uniform mixing temperature as test indicators, the number of intake pipes, the axial angle of the incision, the temperature difference and the diameter of the intake pipe were initially selected as the test indicators. A single-factor simulation performance test analysis was conducted based on Fluent software. The results showed that: the mixing was uniform in the necking section. The degree reaches 75 ~ 80%, and the above factors have a relatively obvious impact on the test indicators.

A test bench was built to conduct a four-factor and five-level quadratic regression orthogonal rotation combined test on the number of intake pipes, incision axial angle, temperature difference and intake pipe diameter. Design-Expert.V8.0.6.1 software was used to optimize the analysis and test indicators. The uniform mixing distance and mixing temperature both meet the requirements of the technical specifications for drying machinery quality evaluation indicators, and the uniform mixing distance is 39.33 mm and the mixing temperature is 50.93°C. The actual data is that the uniform mixing distance is 38.94 mm and the mixing temperature is 51.24°C. The relative errors are respectively are 9.76% and 6.04%, the error between the optimized value and the experimental value is small, and all indicators are at a relatively good level.

ACKNOWLEDGEMENT

This project is supported by the Natural Science Foundation of Heilongjiang Province (LH2022E098).

REFERENCES

[1] Chen, Y.J. (2020). Analysis of my country's food security situation (我国粮食安全形势分析). *Comprehensive agricultural development in China.* Vol.11, pp. 11-14. Beijing/China.

[2] Fahri, O., Mualla, O. Ahmet, B. (2006). Experimental investigations of air and liquid injection by venturi tubes. *Water and Environment Journal*. Vol.20(3), pp. 114-122. United States.

[3] Gao, L.J., Jiang X.X. (2018). Analysis of flow field in water chamber of a certain condenser (某凝汽器水室流场分析). *Mechanical Engineers.* Vol.04, pp. 105-107. Heilongjing/China.

[4] Han, M.L., Zhou.D.K., Chen, X. (2023). Aerodynamic calculation of aircraft external flow field based on FLUENT (基于 FLUENT 的飞行器外流场气动计算). *China high-tech.* Vol. (14). pp. 111-112. Beijing/China.

[5] Hang, Y. (2014). Application of grain drying mechanization technology (谷物干燥机械化技术的应用). *Agricultural technology and equipment.* Vol.01, pp. 42-43. Liaoning/China.

[6] Jiang, F., Hang R. (2022). Analysis of fluid flow characteristics in reducing pipes based on FLUENT (基于 FLUENT 的异径管管内流体流动特性分析). *Welded pipe.* Vol.45(11), pp. 27-30+38. Shanxi/China.

[7] Jiang, S.J., Liu.Q.J. (2009). Research on variable temperature drying technology of rice (稻谷变温干燥工艺研究). *Grain and feed industry.* Vol.02, pp.10-12. Wuhan/China.

[8] Kavga, A., Thomopoulos, V., Pischinas, E., Tsipianitis. D., Nikolakop P. (2023). Design and simulation of a greenhouse in a computational environment (ANSYS/FLUENT) and an automatic control system in a LABVIEW environment. *Simulation Modelling Practice and Theory.* pp. 129. Netherlands.

[9] Li, H. (2019). Design and implementation of improved Venturi fertilizer mixer (改进型文丘里混肥器的设计与实现). *Hebei Agricultural University.* Hebei/China.

[10] Li, H.I. (2019). Experimental research on temperature-variable and quality-preserving drying technology and control process of rice (水稻变温保质干燥工艺及控制过程的试验研究). *Heilongjiang Bayi Agricultural University.* Heilongjing/China.

[11] Liu, C.S., Chen, S.Y., Xiao, S.W., Ma, L.X., Zhang Y., Chen, S. (2023). Technology research and performance verification of rice variable temperature homogeneous drying device (稻谷变温均质干燥装置工艺研究与性能验证). *Journal of Agricultural Machinery.* pp. 366-372. Beijing/China.

[12] Liu, X.H., Xiang Z.L., Tan P., Chen W., Feng J.Y. (2023). Analysis and optimization of internal flow field of heat dissipation system expansion structure based on Fluent (基于 Fluent 的散热系统扩流结构内部流场分析及优化). *Journal of Jilin University (Engineering Edition).* Vol.1-14. pp.10-11. Jilin/China.

[13] Ozkan, F., Ozturk, M., Baylar, A. (2006). Experimental investigations of air and liquid injection by venturi tubes. *Water and Environment Journal.* Vol.20(3). pp. 114-122. England.

[14] Song, K.K., Li, M.Q., Hang, T.C., Song, D.S. (2023). Analysis of solid-liquid mixing performance of integrated mixing and discharge device based on CFD (基于 CFD 的混排一体化装置固液混合性能分析). *Petroleum machinery.* Vol.51(01), pp. 101-139. Hubei/China.

[15] Papkov, V., Shadymov, N., Pashchenko, D. (2023). CFD-modeling of fluid flow in Ansys Fluent using Python-based code for automation of repeating calculations. *International Journal of Modern Physics C*. Vol.34(9). Singapore.